Published in final edited form as:

Anal Chem. 2017 June 20; 89(12): 6440–6447. doi:10.1021/acs.analchem.7b00296.

Multiplexed Lipid Bilayers on Silica Microspheres for Analytical Screening Applications

Nadiezda Fernandez Oropeza[1], **Nesia A. Zurek**[1,*], **Mirella Galvan-De La Cruz**[1], **Aurora Fabry-Wood**[1], **Jennifer M. Fetzer**[1], **Steven W. Graves**[1,2,*], and **Andrew P. Shreve**[1,2,*]

[1]Center for Biomedical Engineering

[2]Department of Chemical and Biological Engineering University of New Mexico Albuquerque, NM 87131

Abstract

Most druggable targets are membrane components, including membrane proteins and soluble proteins that interact with ligands or receptors embedded in membranes. Current target-based screening and intermolecular interaction assays generally do not include the lipid membrane environment in presenting these targets, possibly altering their native structure and leading to misleading or incorrect results. To address this issue, an ideal assay involving membrane components would: 1) mimic the natural membrane environment, 2) be amenable to high-throughput implementation, and 3) be easily multiplexed. In a step towards developing such an ideal target-based analytical assay for membrane components, we present fluorescently indexed multiplexed biomimetic membrane assays amenable to high-throughput flow cytometric detection. We build fluorescently multiplexed biomimetic membrane assays by using varying amounts of a fluorescently labeled lipid, NBD-DOPE, incorporated into a phospholipid membrane bilayer supported on 3 μm silica microspheres. Using flow cytometry, we demonstrate this multiplexed approach by measuring specific affinity of two well characterized systems, the fluorescently labeled soluble proteins Cholera toxin B subunit–Alexa 647 and Streptavidin-PE/Cy5, to membranes containing different amounts of ligand targets of these proteins, GM1 and biotin-DOPE, respectively. This work will enable future efforts in developing highly efficient biomimetic assays for interaction analysis and drug screening involving membrane components.

Introduction

Molecular interactions involving receptors or ligands in cell membranes are essential for cell signaling, transport across membranes, cell-cell recognition, and virus or toxin interactions with cells. As a result, most druggable targets are membrane-associated components, which are of great interest for target-based interaction assays or drug screening.[1–3] Flow cytometry is an attractive method for high-throughput or multiplexed target-based assays, and can quickly investigate interactions or conduct large-scale screens of potential drug candidates.

*Co-corresponding authors: NAZ: nesia505@gmail.com; fax: (505) 277-1979, SWG: graves@unm.edu; fax: (505) 277-1979, APS: shreve@unm.edu; fax: (505) 277-1979.

Conflict of Interest Disclosure

The authors declare no competing financial interest.

[4–10] For example, flow cytometers with automatic sampling methods can rapidly screen high-density microwell plates, where each well contains potentially active compounds and microspheres that present targets.[7] An important element of optimized flow-based assays is the use of multiplexed microspheres so that each sample contains indexed beads that present different targets, as well as positive or negative controls.[4–10] Such multiplexing increases the efficiency of assays by minimizing the cost of the reagents, assay time, and sample-to-sample variability.[7–10] Commercially available sets of polymer microspheres provide high multiplexing capacity (e.g., up to ~500x through combinations of intensity levels and spectral windows), and are widely used for assays involving different types of soluble protein or nucleic acid targets presented through attachment to the particle.[7,11] However, commercially available multiplexed microspheres, which are constructed from polystyrene, are unable to present membrane components in their natural lipid environment.

In general, for interaction analysis involving membrane components, the relevant biological molecules must be presented in either natural or biomimetic membranes, since the structure of membrane components depends on the presence of a lipid bilayer.[1,2,12] A natural membrane environment is also important for functional reasons, including accurate assessment of apparent affinities in multi-valent protein-ligand interactions. For example, the natural interaction of cholera toxin with its GM1 ligand is multi-valent, and the effective affinity is influenced by the lateral mobility of ligands in the membrane.[13]

Substrate-supported membrane bilayers (SMBs), typically formed on silica or modified gold surfaces, are widely used for presentation of membrane components in interaction assays.[14–18] These are the basis of biosensor platforms with transduction of binding events through microscopy, surface plasmon resonance, ellipsometry, second harmonic generation, or quartz crystal microbalance response.[13,19–25] Unfortunately, while planar SMBs mimic many aspects of natural cellular membranes, including incorporation of membrane proteins, they are difficult to integrate with highly multiplexed methods. Some work has developed patterned SMBs that contain different regions of membrane composition,[26–30] possibly allowing for multiple target presentation, but even for low-throughput applications their use for assays requires complex surface patterning and fluidic engineering.[29–31]

Motivated by these considerations, there is interest in producing a lipid bilayer membrane architecture that will enable multiplexed and high-throughput flow cytometry. Liposomes are one possibility, as membrane components can be readily integrated with them, and they can, in principle, be labeled for multiplexed indexing.[32] However, typical liposomes of sizes ~200 nm or smaller are challenging to analyze using flow cytometry, and for assays, analytical limitations also arise from the mismatch between the size of the analyte particle and the interrogation volume.[33,34] Giant unilamellar vesicles (GUVs), several microns or larger in size, are another alternative amenable to incorporation of membrane components.[35,36] Further investigation of GUVs in this context is warranted, but to date, GUVs have only rarely been used as a platform for flow cytometry, in part because of complications arising from structural and size heterogeneities.[37,38]

An ideal platform for multiplexed flow-based studies of membrane components would incorporate the best features of vesicles and particle-based multiplexing methods. Our work

presents an initial step toward that goal, relying upon SMBs formed on silica microspheres. Monodisperse silica microspheres are commercially available and are easily detected and analyzed using flow cytometry. SMBs on silica microspheres are used for flow-based assays and are similar to SMBs on planar silica in membrane quality.[39–43] However, to date, no studies have demonstrated multiplexing methods for SMBs on silica microspheres, and there are no readily available sources of standardized multiplexed silica particles optimized for use in flow cytometry.

As a proof-of-principle demonstration of multiplexing methods for membrane components in flow cytometry, we present measurements that rely upon use of different amounts of fluorescently tagged lipids incorporated into SMBs on silica microspheres to index the particles. Each type of indexed particle presents a lipid membrane of different composition. For the experiments reported here, each membrane contains different amounts of lipid-based small molecule ligands that bind to the fluorescently labeled proteins cholera toxin (B subunit) and streptavidin. These two systems have been widely studied and offer well characterized test cases to validate the multiplexing technology we are developing.[13,22–25,44] This work demonstrates technology for multiplexed membrane-based assays in flow cytometry, and represents an initial step toward building more efficient analysis methods for membrane-associated components.

Materials and Methods

Liposome Preparation.

Liposomes were prepared as previously reported.[45] Briefly, powdered 1-palmitoyl-2-oleoyl-sn-glycero-3-phosphocholine (POPC), 1,2-dioleoyl-sn-glycero-3phosphoethanolamine-N-(biotinyl) (biotin-DOPE), 1,2-dioleoyl-sn-glycero-3phosphoethanolamine-N-(7-nitro-2–1,3-benzoxadiazol-4-yl) (NBD-DOPE), and Ganglioside GM1 purchased from Avanti Lipids were dissolved in chloroform (EMD Millipore) and stored in glass vials at −20°C until use. Using glass syringes, stock lipids were mixed in different glass vials in various final mixtures. The mixtures of chloroform-dissolved lipids were dried overnight under vacuum to form lipid plaques. The lipid plaques were then rehydrated to a final concentration of 1 mM in phosphate buffered saline (PBS, Sigma) at pH 7.4. Large unilamellar vesicles (LUVs) were formed by extrusion using the Mini-Extruder, filter supports, and 0.1 μm polycarbonate (PC) membranes (Avanti Polar Lipids) by passing rehydrated lipids through the PC membranes 13 times.

Microsphere Supported Bilayer Formation.

All Eppendorf tubes were passivated with 0.1 mg/mL Bovine Serum Albumin (BSA) for 45 minutes prior to use. 3 μm non-porous silica microspheres purchased from Spherotech were cleaned by first suspending them in a basic solution (4% NH_4OH), followed by slow centrifugation and rinsing with Millipore water 3 times. Next, the beads were suspended in an acidic solution (4% HCl), followed by slow centrifugation and rinsing with Millipore water 5 times.[43] Cleaned beads were suspended in PBS. The silica beads were coated with a lipid bilayer as previously described, with some modifications.[43] Briefly, the silica beads (1.5 μL of suspended beads) were added to the LUVs (1 mM lipid concentration) to a final

concentration ~10^6 beads/mL in 0.5 mL final volume. The mixture of LUVs and microspheres was vortexed on high speed at room temperature for 10 minutes and on low speed for 45 minutes at 37 °C. Under these conditions, liposomes fuse to the surface, forming a uniform supported lipid bilayer.[46] As a precaution to minimize non-specific binding, BSA was then added to samples at a concentration of 0.5 mg/mL and the samples were vortexed on low speed at room temperature for 45 minutes. Beads were then washed 4–5X to remove unbound liposomes by cycles of centrifugation at 10,000 rpm for 45 seconds, followed by removing the supernatant, always leaving at least 50 μL in the tube to keep the lipid coated beads hydrated. Beads were re-suspended in fresh PBS to bring the samples back up to volume. A multiplexed set was formed by mixing beads coated with different membrane compositions in a BSA-passivated tube. Following rinsing, resuspension, and addition of analyte solution (see below), the final bead concentration for analysis was ~10^5 beads/mL.

Protein Binding Assays.

Cholera Toxin B subunit (recombinant) – Alexa Fluor 647 (CTxB-Alexa 647) purchased from ThermoFisher at a concentration of 175 nM was diluted to a stock concentration of 75 nM in PBS and stored in aliquots at −20˚C until use. Streptavidin-PE/Cy5 (SAv-Cy5) diluted in PBS purchased from Biolegend at a concentration of 421 nM was diluted in PBS to a stock concentration of 4.21 nM and stored in aliquots at −20˚C until use. Concentrations of GM1, CTxB-Alexa 647, biotin-DOPE and SAv-Cy5 were chosen based on previous literature.[13,23,44] POPC membrane bilayers containing specific amounts of GM1 (0 to 0.5 mol%) or biotin-DOPE (0 to 0.5 mol%), and as appropriate, NBD-DOPE (0 to 2.0 mol%) as a fluorescent indexing label, were prepared on silica microspheres as single samples or, by mixing the single samples, as multiplexed sets. From microsphere size, concentration and the membrane compositions, the maximum concentration of protein binding sites is estimated to be of order 10^{-11} Molar. Different amounts of CTxB-Alexa 647 (0 to 20 nM) and/or SAv-Cy5 (0 to 2.5 nM) were added in solution to both single samples and multiplexed samples and incubated for 10 minutes before analysis. A multiplexed cross-reactivity assay was also performed on silica microspheres coated with the following lipid compositions: 1) 100 mol% POPC; 2) 0.5 mol% GM1, 0.2 mol% NBD-DOPE and 99.7 mol % POPC; 3) 0.5 mol% biotin-DOPE, 2 mol% NBD-DOPE and 97.5 mol% POPC. Different proteins (2.5 nM SAv-Cy5; 20 nM CTxB-Alexa Fluor 647; or the combination of 2.5 nM SAv-Cy5 *and* 20 nM CTxB-Alexa) were added in solution to the multiplexed beads and incubated for 10 minutes before analysis.

Flow Cytometry.

Flow cytometric studies were done as previously described using an Accuri C6 flow cytometer, with minor modifications to the protocol.[47] This instrument has two lasers with independent optical paths (488 nm and 640 nm) and four fluorescence detectors (three from the 488 nm excitation line – FL-1: 533 nm center wavelength/30 nm bandpass, FL-2: 585 nm center wavelength/40 nm bandpass, and FL-3: 670 nm longpass emission; and one from the 640 nm excitation line – FL-4: 675 nm center wavelength/25 nm bandpass emission). For convenience, we sometimes describe filters using the center wavelength and bandpass, so for example, FL-1 corresponds to 533/30. For each event, data were collected for forward

scatter (FSC) and side scatter (SSC) (from the 488 nm laser) and all four fluorescence channels. The Accuri C6 was calibrated with eight-peak rainbow beads (Spherotech, Inc.) and fluorescence data were quite stable over time, as gauged by coefficient of variation (CV) values. The instrument was back-flushed between sample types and the system was cleaned and decontaminated after each use. Collected data were analyzed, gated, and compensated as necessary using FlowJoV10 software. Bivariate flow cytometry data are presented as 10% contour levels of the probability density of events, with additional points representing (outlying) events that occur outside the lowest 10% probability contour. Red lines indicate gates that show populations selected for quantitative analysis. Median fluorescence intensity measurements were obtained using FlowJoV10 and data were analyzed and plotted using Microsoft Excel, Matlab or Igor Pro software.

Results and Discussion

Fluorescently Indexed Silica Microsphere Supported Lipid Bilayers.

Multiplexed flow cytometry allows researchers to include several different samples, including controls, in each sample well prior to screening.[4–10] This approach decreases sample-to-sample variation and lowers reagent cost. In this proof-of-principle study, we use fluorescently tagged lipids to provide different fluorescent intensity levels to index 3 μm silica microspheres. To test this approach, we coat silica microspheres in lipid mixtures containing 100% POPC, 99.8% POPC + 0.2% NBD-DOPE, or 98% POPC + 2% NBD-DOPE. Next, we rinse the microspheres and combine the three samples into a single tube to build a fluorescently indexed multiplex set (Figure 1A).

Flow Cytometric Characterization.

We analyze fluorescently indexed microspheres by flow cytometry (Figures 1B and 1C). The population of events is gated using side scatter (Figure 1B, y-axis) versus forward scatter (Figure 1B, x-axis) and the automated gating function in FlowJoV10 (Figure 1B, red line). Signals from the events selected in Figure 1B are plotted on a bivariate plot of side scatter (Figure 1C, y-axis) versus green fluorescence (FL-1) (Figure 1C, x-axis), and the three different microsphere populations in the multiplexed system are clearly identifiable. When the fluorescence of the multiplexed silica microspheres is tracked over time, the signal intensities are stable over sufficiently long times for typical assay measurements (in our case, assay times up to 30 minutes were used), and the stability of the fluorescence intensities is comparable to that of the individual samples used to generate the multiplexed samples (Supporting Figure S1). These data show that we produce fluorescently indexed silica microspheres bearing lipid bilayers by varying the amounts of NBD-DOPE lipids in each single sample, and that a multiplexed sample is made when these microspheres are combined.

Multiplexed Protein Binding Assays.

Fluorescently indexed microspheres coated with different concentrations of GM1 in POPC membrane bilayers show differential binding of CTxB–Alexa 647, a protein with a multi-valent association with the glycolipid GM1 ligand.[13] Silica microspheres are coated with increasing concentrations of GM1 and NBD-DOPE (100% POPC, 99.75 POPC

+ 0.05%GM1 + 0.2% NBD-DOPE, or 97.5% POPC + 0.5% GM1 + 2% NBD-DOPE), building a fluorescently multiplexed bead set to test the affinity of CTxB-Alexa 647 to GM1-containing membranes. Next, different concentrations of CTxB-Alexa 647 ranging from 0 nM to 20 nM are added to both the individual samples and the multiplexed sample and analyzed after a 10 minute incubation. The event population is first gated using a forward scatter versus side scatter plot, as in Figure 1B, which selects a population of microspheres. Then, data from the selected events are shown on a bivariate plot of FL-4 channel intensity (excitation: 640nm, emission: 675/25nm; CTxB-Alexa 647 detection channel; Figure 2, y-axis) versus FL-1 channel intensity (excitation: 488nm, emission: 533/30nm; NBD-DOPE multiplexing channel; Figure 2, x-axis). From this plot, gates are further refined to include only well-coated microspheres, excluding other debris or particles with poorly formed membranes (Figure 2, red gates). When no CTxB-Alexa 647 is added to either the individual or multiplexed samples (0 nM CTxB-Alexa 647), the FL-4 fluorescence intensity does not change (Figure 2A, E, I, and M), consistent with no CTxB-Alexa 647 binding.

Results from the addition of increasing concentrations of CTxB-Alexa 647 to samples with no GM1 (Figure 2A-D) indicate little non-specific binding of CTxB-Alexa 647 for the main population of microspheres. However, a small sub-population of events does show an increase in FL-4 signal, as would be observed for non-specific interactions of CTxB-Alexa 647 with microspheres containing no GM1. A likely origin of this sub-population is apparent by inspection of the bivariate FL-4 versus FL-1 plots for the cases where DOPE-NBD is present (0.2% or 2.0% GM1 columns, Figure 2E-H and 2I-L, respectively). In these cases, a broadening of the population distribution toward lower FL-1 intensity coinciding with FL-4 intensity above background level is consistent with non-specific binding of CTxB-Alexa 647 to a sub-population of microspheres that have non-uniform or incomplete lipid coating. This result is also consistent with the observation (data not shown) that some concentration-dependent non-specific binding of CTxB-Alexa 647 to bare silica microspheres occurs. Gating of the bivariate data to retain only the main populations of microspheres, those with well-formed lipid membranes, removes much of this complicating non-specific interaction effect, illustrating a powerful aspect of multi-variate flow cytometry analysis of interactions of proteins and membranes. An increase of fluorescence in FL-4 in single composition beads with higher concentrations of GM1 indicates that CTxB-Alexa 647 interacts specifically with GM1 (Figure 2E-L). Separate control experiments confirm the absence of concentration-dependent CTxB-Alexa 647 binding to NBD-DOPE on particles with well-formed membranes when no GM1 is present (Supporting Figure S2).

In the multiplexed set with three fluorescently indexed bead populations in a single tube, higher fluorescence in the multiplexing channel (FL-1; NBD-DOPE) is matched to increasing GM1 content in the membrane (Figure 2M-P). Specifically, when increasing concentrations of CTxB-Alexa 647 are added to multiplexed samples, the FL-4 signal increases for beads with membranes that contain more GM1 (Figure 2M-P), consistent with binding of CTxB-Alexa 647 to GM1. The bead population with no GM1 in its membranes maintains low binding of CTxB-Alexa 647 (Figure 2M-P, red arrows). Overall, these data indicate the specific binding of CTxB-Alexa 647 to GM1 in a multiplex format.

The median FL-4 signal of the main bead populations (e.g., Figure 2 M-P, red gates) is used to measure the amount of CTxB-Alexa 647 bound to microspheres. A multiplexed data set thus consists of the median FL-4 signal of each microsphere population as a function of CTxB-Alexa 647 concentration. Each microsphere population corresponds to a different GM1 concentration, so a full multiplexed data set provides the amount of CTxB-Alexa 647 bound to microspheres as a function of both CTxB-Alexa 647 concentration (different panels of Figure 2 M-P) and GM1 concentration (different populations within each panel). For each GM1 concentration, the median FL-4 signal, S, as a function of CTxB-Alexa 647 concentration, [CTxB], is fit to a first-order Hill Equation including background, B:

$$S = B + (M - B)\left(\frac{K_{eff}[\text{CTxB}]}{1 + K_{eff}[\text{CTxB}]}\right) \quad (1)$$

In Equation (1), K_{eff} is an effective association constant and M is the maximum signal predicted by the model. For each data set from a population of microspheres, this fit yields values of B, M and K_{eff} for the GM1 concentration of those microspheres. Then, using the value of M obtained for the maximum GM1 concentration of 0.5 mol%, designated $M_{0.5}$, a normalized fractional signal for each data set is generated as:

$$f = \frac{S - B}{M_{0.5} - B} = \frac{K_{eff}[\text{CTxB}]}{1 + K_{eff}[\text{CTxB}]} \quad (2)$$

where f is the fraction of the maximum amount of CTxB-Alexa 647 binding that occurs for GM1 membrane concentration of 0.5 mol%. This normalization process generates a family of curves for each complete multiplexed and individual data set. Four complete replica experiments are analyzed, and the f values are averaged and plotted to produce binding data (Figure 3).

Two major results are found. First, the multiplexed approach agrees well with the results of individual samples. In fact, fitting of the four data sets in Figure 3 that correspond to non-zero values of GM1 concentration (red and blue curves of the upper and lower panels) provides values of K_{eff} with 95% confidence intervals that all overlap. More detailed analysis is unwarranted, given the small number of degrees of freedom in the nonlinear regression models. Averaging the two values of K_{eff} obtained from the multiplex fits yields a value of $K_{eff} = 0.25 \pm 0.12$ nM^{-1}, corresponding to an effective or apparent affinity of $1/K_{eff} = 4.0 \pm 1.9$ nM, where the reported uncertainties are 95% confidence intervals. Second, the multiplex results found here are also in agreement with previously published work. A detailed study by Lauer et al. presented a complete analysis of the multi-valent interaction of cholera toxin with GM1, describing both single-site binding interactions and enhancement of apparent affinity through surface avidity.[13] These authors report an effective affinity of approximately 5 nM, which agrees with our result. They also report the single-site affinity of GM1 for cholera toxin to be several hundred times weaker. Their model demonstrates that observation of nanomolar effective affinity is consistent with multi-valent cholera-GM1 interaction arising from the presentation of GM1 in a laterally fluid membrane. Our results

thus confirm that the important lateral fluidity function of natural membranes is maintained in the multiplex assay.

To further validate the multiplexed detection approach, we also present protein binding assays using biotin-DOPE lipids and Streptavidin-PE/Cy5 (abbreviated as SAv-Cy5). Silica microspheres coated with lipid mixtures containing varying concentrations of biotinylated-DOPE and NBD-DOPE (100% POPC, 99.75% POPC + 0.05% Biotin-DOPE + 0.2% NBDDOPE, or 97.5% POPC + 0.5% Biotin-DOPE + 2.0% NBD-DOPE) are combined into a multiplexed set. Different concentrations of SAvCy5 from 0 nM to 2.5 nM are added to the multiplex, incubated for 10 minutes, and flow cytometry data are collected. For the fluorophores used in this study, there is some spectral overlap in the FL-1 (NBD-DOPE detection) and FL-3 (SAv-Cy5 detection) channels. Therefore, flow cytometric data compensation methods are applied (Supporting Figure S3).[48] Following compensation, bead populations are plotted on bivariate plots of FL-3 versus FL-1 intensities, gates are drawn around the main bead populations, and median fluorescence intensities in FL-3 are obtained using FlowJoV10 (Supporting Figure S4, red gates). Analysis of the median fluorescence FL-3 signal intensity is performed using a similar procedure to that outlined above for four replicate. experiments.

Figure 4 presents results for both multiplexed and individual samples. In both cases, the median FL-3 signal increases slightly at high concentrations of SAv-Cy5 even when no biotin-DOPE is present, indicating some non-specific binding of SAv-Cy5 to the beads (Figure 4, lowest curves). However, separate control experiments confirm the absence of any additional specific interaction of SAv-Cy5 with the multiplexing label NBD-DOPE when no biotin-DOPE is present (Supporting Figure S5). In this example, the appreciable non-specific binding of SAvCy5 to beads with no biotin-DOPE and the increased specific binding to beads containing biotin-DOPE in the multiplexed set demonstrates the power of multiplexed analysis. The multiplexed sample contains all three biotin compositions and a single SAv-Cy5 concentration, thus reducing sample-to-sample variability in quantitative determination of specific and non-specific responses. As for the case of CTxB-Alexa 647 interaction with GM1, similar quantitative behavior in the individual and multiplex samples confirms that fluorescently indexed membrane coated silica microspheres provide a reliable alternative to individual bead-based measurements.

A similar analysis to that described above was carried out for the concentration dependent binding data presented in Figure 4. The 95% confidence intervals of all the effective affinities again overlap, and when averaged, the resulting effective affinity of the two multiplexed results is $1/K_{eff} = 2.1 \pm 1.6$ nM (reported uncertainty is the 95% confidence interval). The apparent affinity of streptavidin association with biotin-presenting surfaces has been treated in detail by several investigators.[23,44] Again, our goal is to demonstrate that the multiplexed approach provides an accurate assessment of the effective affinity for the chosen experimental conditions. To that end, our results are similar to previous reports of an apparent affinity of ~2.3 nM by Nguyen et. al. or, for biotin covalently attached to surfaces, of ~6 nM by Seto et. al.,[23,44] providing additional evidence that the mulitplexed approach produces accurate assessments of effective interactions involving membrane components.

Binding Specificity in Multiplexed Protein Binding Assays.

For realistic multiplexed applications, each sample should contain beads with different membrane components, and not just different concentrations of a single component. To verify that we can use silica microspheres with different membrane components in a single well, we coat the particles with membranes of 100% POPC (negative control), 0.5% GM1 and 0.2% NBD-DOPE (to bind CTxB–Alexa 647), or 0.5% biotin-DOPE and 2% NBD-DOPE (to bind SAv-Cy5). The three fluorescently indexed membrane-coated silica microspheres are mixed into a single tube, and 20 nM CTxB-Alexa 647 and 2.5 nM SAv-Cy5 are added to assess the binding specificity of each protein to membrane components. Flow cytometry data is collected and analyzed as before, with compensation applied to account for partial overlap of the FL-3 channel with both FL-1 and FL-4 signals (Supporting Figure S6). The bead population of each multiplexed sample is gated as in Figure 1B and plotted on bivariate plots of FL-4 (Figure 5A-D) or FL-3 (Figure 5E-H) versus FL-1. In samples where neither protein is added, FL-3 and FL-4 signals are low (Figure 5A and 5E). In the presence of 20 nM CTxB-Alexa 647, fluorescence is low on all bead populations in the FL-3 channel (Figure 5F) but increases in the FL-4 channel on the bead population containing 0.5% GM1 (Figure 5B). These results show specific binding of CTxB-Alexa 647 to GM1. When 2.5 nM SAv-Cy5 is added, the fluorescence intensity in the FL-3 channel increases on the bead population containing 0.5% biotin-DOPE (Figure 5G). Fluorescence also increases slightly on the other bead populations in the FL-3 channel (Figure 5G), showing non-specific binding of SAv-Cy5 to other lipid compositions as discussed previously. There is also a small increase in FL-4 fluorescence in the sample containing SAv-Cy5 (Figure 5C), attributed to Cy5 fluorescence spillover into the FL-4 channel. When both 20 nM CTxB- Alexa 647 and 2.5 nM SAv-Cy5 are added, FL-4 fluorescence increases substantially on the bead population containing GM1, slightly on the population containing biotin-DOPE (indicating non-specific binding), and not on the population containing 100% POPC (Figure 5D), indicating the absence of any additional nonspecific binding beyond that observed in Figure 5C. Additionally, fluorescence in the FL-3 channel increases similarly to the sample containing only SAv-Cy5, indicating specific binding of the SAv-Cy5 to biotin-DOPE (Figure 5H). The median intensities in FL-4 and FL-3 corresponding to the gated data from Figure 5, averaged over four replicate experiments, are shown in Supporting Figure S7.

Conclusion

Our results demonstrate the use of multiplexed microsphere-based assays for differential binding assays that involve membrane components. These methods are similar to those required for screening applications. While we have presented a small multiplex, expansion to large multiplexed sets (n ~ 100 or larger) should be possible using strategies similar to those implemented for polymer-based indexed microspheres.[7] To achieve that long-term goal in a commercially viable implementation, one of two materials development paths can be followed. Since supported membrane bilayers on silica microspheres are readily produced, one approach is to develop reliable labeling strategies to index silica microspheres without altering the surface chemistry needed for stable membrane assembly. An alternative approach is to develop well-characterized model membranes on commercially available highly multiplexed polymer microspheres. To conclude, our results show that fluorescently

indexed membranes on silica microspheres enable multiplexed differential binding assays using flow cytometry. For two test cases, the mulitplexed methods we present yield results in good agreement with prior studies. Overall, this study provides an initial step to building multiplexed high-throughput flow cytometry assays involving membrane-associated components. Continued development of this multiplexed lipid membrane platform will occur through investigation of methods to generate larger multiplexed sets of targets and controls, and in applications of this technology to flow-cytometry-based interaction analysis or screening studies.

Supplementary Material

Refer to Web version on PubMed Central for supplementary material.

Acknowledgments

APS, SWG and JF were supported by NIH R21 EB016339. NAZ was supported for a portion of this work for training opportunities through the New Mexico Cancer Nanotechnology Training Center CA-R25153825. AFW and SWG were also supported in part by NSF 1318833, NSF 1518861 and NIH R21 AI115105. MGD was funded by UNM-IMSD/NIH GM060201. Some data were generated in the UNM Shared Flow Cytometry and High Throughput Screening Resource Center supported by the University of New Mexico Health Sciences Center and the University of New Mexico Cancer Center with current funding from NCI 2P30 CA118100–11 “UNM Cancer Center Support Grant”.

References

(1). Yin H; Flynn AD Annu. Rev. Biomed. Eng 2016, 18, 51–76. [PubMed: 26863923]

(2). Allen JA; Roth BL Annu. Rev. Pharmacol. Toxicol 2011, 51, 117–144. [PubMed: 20868273]

(3). Overington JP; Al-Lazikani B; Hopkins AL Nat Rev Drug Discov 2006, 5, 993–996. [PubMed: 17139284]

(4). Vignali DA A. J. Immunol. Methods 2000, 243, 243–255. [PubMed: 10986418]

(5). Kellar KL; Iannone MA Exp. Hematol 2002, 30, 1227–1237. [PubMed: 12423675]

(6). Kellar KL; Douglass JP J. Immunol. Methods 2003, 279, 277–285. [PubMed: 12969567]

(7). Edwards BS; Sklar LA J. Biomol. Screen 2015, 20, 689–707. [PubMed: 25805180]

(8). Saunders MJ; Edwards BS; Zhu J; Sklar LA; Graves SW Curr. Protoc. Cytom 2010, Chapter 13, Unit 13.12.1–17.

(9). Simons PC; Young SM; Carter MB; Waller A; Zhai D; Reed JC; Edwards BS; Sklar LA Nat. Protoc 2011, 6, 943–952. [PubMed: 21720309]

(10). Edwards BS; Zhu JS; Chen J; Carter MB; Thal DM; Tesmer JJG; Graves SW; Sklar LA Cytom. Part A 2012, 81A (5), 419–429.

(11). Yu C; Mannan AM; Yvone GM; Ross KN; Zhang Y-L; Marton MA; Taylor BR; Crenshaw A; Gould JZ; Tamayo P; Weir BA; Tsherniak A; Wong B; Garraway LA; Shamji AF; Palmer MA; Foley MA; Winckler W; Schreiber SL; Kung AL; Golub TR Nat Biotech 2016, 34, 419–423.

(12). Tiefenauer L; Demarche S Materials (Basel) 2012, 5, 2205–2242.

(13). Lauer S; Goldstein B; Nolan RL; Nolan JP Biochemistry 2002, 41, 1742–1751. [PubMed: 11827518]

(14). Sackmann E Science (80-.) 1996, 271, 43–48.

(15). Heyse S; Ernst OP; Dienes Z; Hofmann KP; Vogel H Biochemistry 1998, 37, 507–522. [PubMed: 9425071]

(16). Plant AL Langmuir 1993, 9, 2764–2767.

(17). Wagner ML; Tamm LK Biophys. J 2000, 79, 1400–1414. [PubMed: 10969002]

(18). Diaz AJ; Albertorio F; Daniel S; Cremer PS Langmuir 2008, 24, 6820–6826. [PubMed: 18510376]

(19). Plant AL Langmuir 1999, 15, 5128–5135.
(20). Song X; Swanson BI Anal. Chim. Acta 2001, 442, 79–87.
(21). Shreve AP; Howland MC; Sapuri-Butti AR; Allen TW; Parikh AN Langmuir 2008, 24, 13250–13253. [PubMed: 19007257]
(22). Jung H; Robison AD; Cremer PS J. Struct. Biol 2009, 168, 90–94. [PubMed: 19508894]
(23). Nguyen TT; Sly KL; Conboy JC Anal. Chem 2011, 84, 201–208. [PubMed: 22122646]
(24). Worstell NC; Krishnan P; Weatherston JD; Wu H-J PLoS One 2016, DOI: 10.1371/journal.pone.0153265.
(25). Tran RJ; Sly KL; Conboy JC Annu. Rev. Anal. Chem 2017, 10:11.1–11.28.
(26). Nair PM; Salaita K; Petit RS; Groves JT Nat. Protoc 2011, 6, 523–539. [PubMed: 21455188]
(27). Oliver AE; Kendall EL; Howland MC; Sanii B; Shreve AP; Parikh AN Lab Chip 2008, 8, 892–897. [PubMed: 18497908]
(28). Yang T-HC; Yee CK; Amweg ML; Singh S; Kendall EL; Dattelbaum AM; Shreve AP; Brinker CJ; Parikh AN Nano Lett 2007, 7, 2446–2451. [PubMed: 17629349]
(29). Smith KA; Gale BK; Conboy JC Anal. Chem 2008, 80, 7980–7987. [PubMed: 18841940]
(30). Chao L; Daniel SJ Am. Chem. Soc 2011, 133, 15635–15643.
(31). Costello DA; Millet JK; Hsia C-Y; Whittaker GR; Daniel S Biomaterials 2013, 34, 7895–7904. [PubMed: 23886734]
(32). Beloglazova NV; Goryacheva OA; Speranskaya ES; Aubert T; Shmelin PS; Kurbangaleev VR; Goryacheva IY; De Saeger S Talanta 2015, 134, 120–125. [PubMed: 25618647]
(33). Friedrich R; Block S; Alizadehheidari M; Heider S; Fritzsche J; Esbjorner EK; Westerlund F; Bally M Lab Chip 2017, 17, 830–841. [PubMed: 28128381]
(34). Piyasena ME; Graves SW Lab Chip 2014, 14, 1044–1059. [PubMed: 24488050]
(35). Czogalla A; Grzybek M; Jones W; Coskun Ü Biochim. Biophys. Acta 2014, 1841, 1049–1059. [PubMed: 24374254]
(36). Jørgensen IL; Kemmer GC; Pomorski TG Eur. Biophys. J 2017, 46, 103–119. [PubMed: 27437691]
(37). Nishimura K; Hosoi T; Sunami T; Toyota T; Fujinami M; Oguma K; Matsuura T; Suzuki H; Yomo T Langmuir 2009, 25, 10439–10443. [PubMed: 19670878]
(38). Nishimura K; Matsuura T; Nishimura K; Sunami T; Suzuki H; Yomo T Langmuir 2012, 28, 8426–8432. [PubMed: 22578080]
(39). Zeineldin R; Piyasena ME; Sklar LA; Whitten D; Lopez GP Langmuir 2008, 24, 4125–4131. [PubMed: 18302435]
(40). Conway JW; Madwar C; Edwardson TG; McLaughlin CK; Fahkoury J; Lennox RB; Sleiman HF J. Am. Chem. Soc 2014, 136, 12987–12997. [PubMed: 25140890]
(41). Gopalakrishnan G; Rouiller I; Colman DR; Lennox RB Langmuir 2009, 25, 5455–5458. [PubMed: 19382772]
(42). Piyasena ME; Zeineldin R; Fenton K; Buranda T; Lopez GP Biointerphases 2008, 3, 38. [PubMed: 20408688]
(43). Buranda T; Huang J; Ramarao GV; Ista LK; Larson RS; Ward TL; Sklar LA; Lopez GP Langmuir 2003, 19, 1654–1663.
(44). Seto H; Yamashita C; Kamba S; Kondo T; Hasegawa M; Matsuno M; Ogawa Y; Hoshino Y; Miura Y Langmuir 2013, 29, 9457–9463. [PubMed: 23808479]
(45). Werner JH; Montaño GA; Garcia AL; Zurek NA; Akhadov EA; Lopez GP; Shreve AP Langmuir 2009, 25, 2986–2993. [PubMed: 19437708]
(46). Silva-López EI; Edens LE; Barden AO; Keller DJ; Brozik JA Chem. Phys. Lipids 2014, 183, 91–99. [PubMed: 24911903]
(47). Corbitt TS; Zhou Z; Tang Y; Graves SW; Whitten DG ACS Appl. Mater. Interfaces 2011, 3, 2938–2943. [PubMed: 21714540]
(48). Herzenberg LA; Tung J; Moore WA; Herzenberg LA; Parks DR Nat. Immunol 2006, 7, 681–685. [PubMed: 16785881]

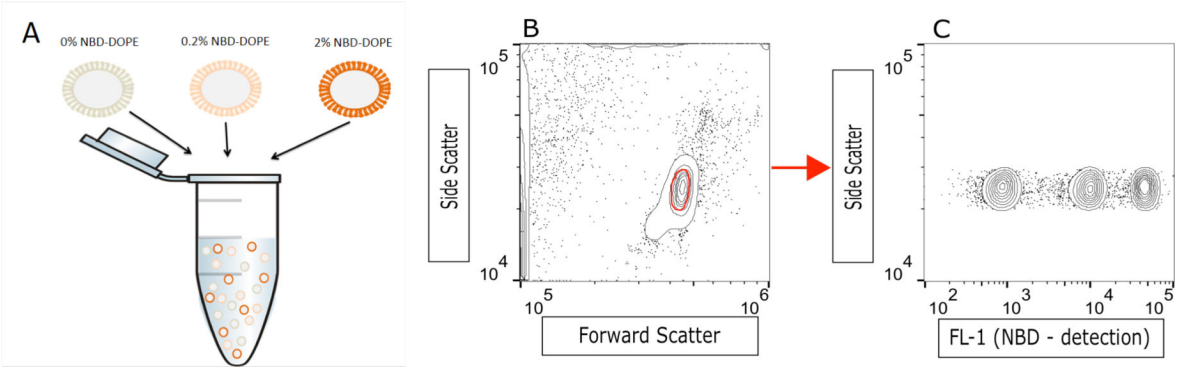

Figure 1.

A) Schematic of supported lipid bilayers on non-porous silica microspheres. The microspheres are fluorescently indexed by coating them with different concentrations of fluorescently labeled lipids, 100% POPC, 99.8% POPC and 0.2% NBD-DOPE, and 98% POPC and 2% NBD-DOPE. The coated microspheres are then rinsed and combined in a microfuge tube to build a multiplexed set of lipid-coated microspheres. Multiplex systems can be used for membrane-based assays such as membrane composition dependent protein binding. **B,C)** Analysis and gating of fluorescently indexed membrane-coated microspheres in a triplex system. Side scatter versus forward scatter data (Panel B) are used to gate or select events that correspond to microspheres (red circle in Panel B, see text), and data from the gated events are then plotted as side scatter versus FL-1 (excitation laser 488 nm, emission filter 533/30) intensity in Panel C. Similar approaches are used in later experiments to detect protein binding to surfaces of different lipid compositions.

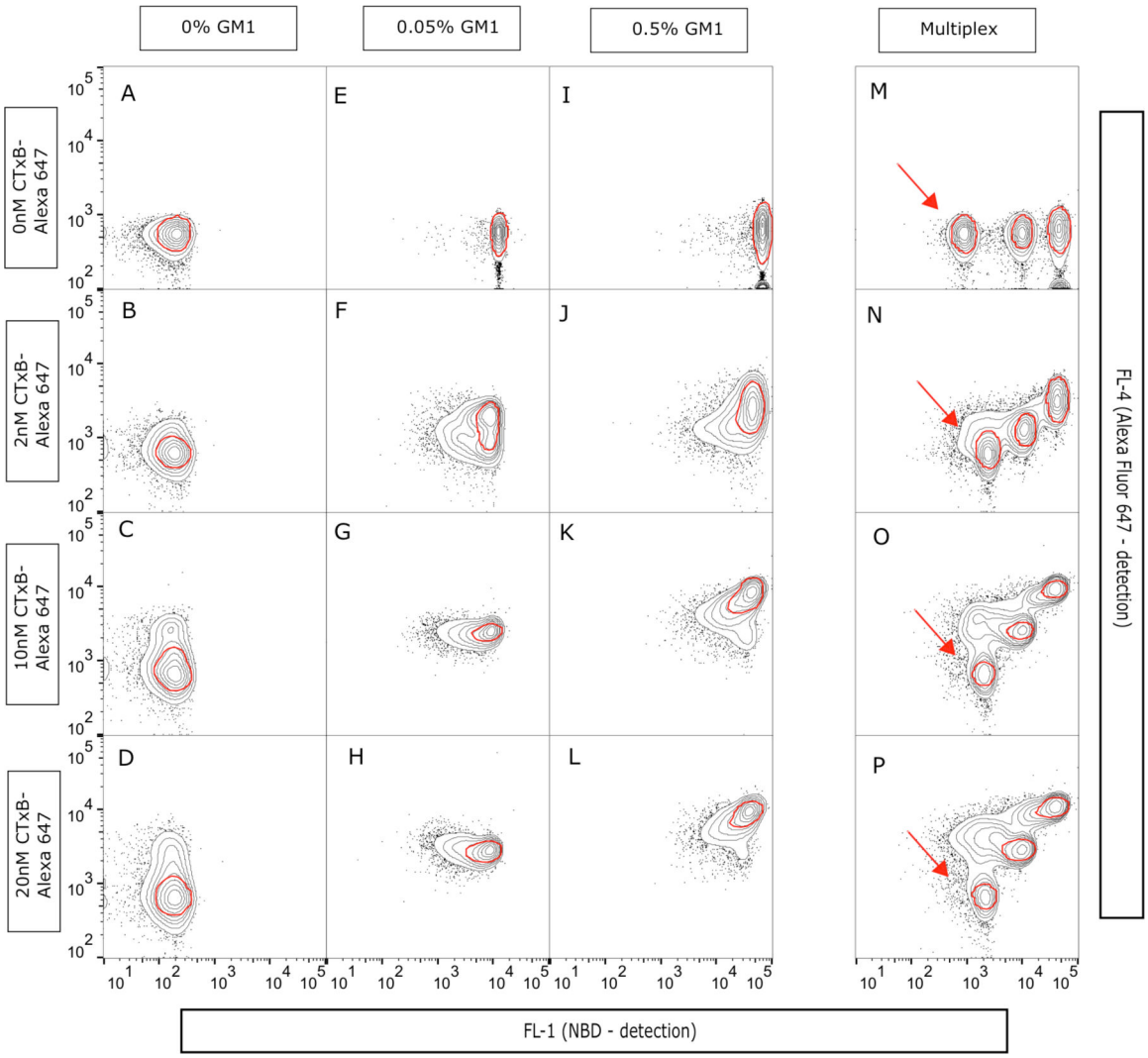

Figure 2.

Bivariate contour plots (FL-4 vs. FL-1). Individual samples: 0 mol% GM1: **A**) Plus 0 nM CTxB-Alexa 647. **B**) Plus 2 nM CTxB-Alexa 647. **C**) Plus 10 nM CTxB-Alexa 647. **D**) Plus 20 nM CTxB-Alexa 647. 0.05 mol% GM1: **E**) Plus 0 nM CTxB-Alexa 647. **F**) Plus 2 nM CTxB-Alexa 647. **G**) Plus 10 nM CTxB-Alexa 647. **H**) Plus 20 nM CTxB-Alexa 647. 0.5 mol% GM1: **I**) Plus 0 nM CTxB-Alexa 647. **J**) Plus 2 nM CTxB-Alexa 647. **K**) Plus 10 nM CTxB-Alexa 647. **L**) Plus 20 nM CTxB-Alexa 647. Multiplexed samples: **M**) Plus 0 nM CTxB-Alexa 647. **N**) Plus 2 nM CTxB-Alexa 647. **O**) Plus 10 nM CTxB-Alexa 647. **P**) Plus 20 nM CTxB-Alexa 647.

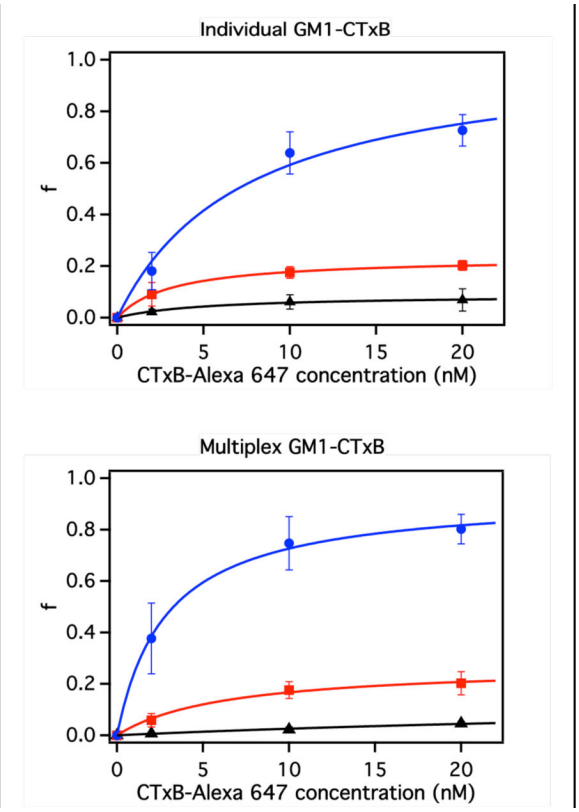

Figure 3.

Fractional binding of cholera toxin (CTxBAlexa 647) after 10 minutes of incubation of samples containing lipids with 100% POPC + 0% GM1 (black, triangles), 99.75% POPC + 0.2% NBD-DOPE + 0.05% GM1 (red, squares) and 97.5% POPC + 2% NBD– DOPE + 0.5% GM1 (blue, circles). The x-axis is concentration of CTxB-Alexa 647 added to the system. Data shown are the average of four replicates, and error bars are plus/minus one standard deviation. Solid lines are fits to the averaged data following the functional form of Equation (2). The top panel presents results from individual samples, while the bottom panel presents results from the multiplex system.

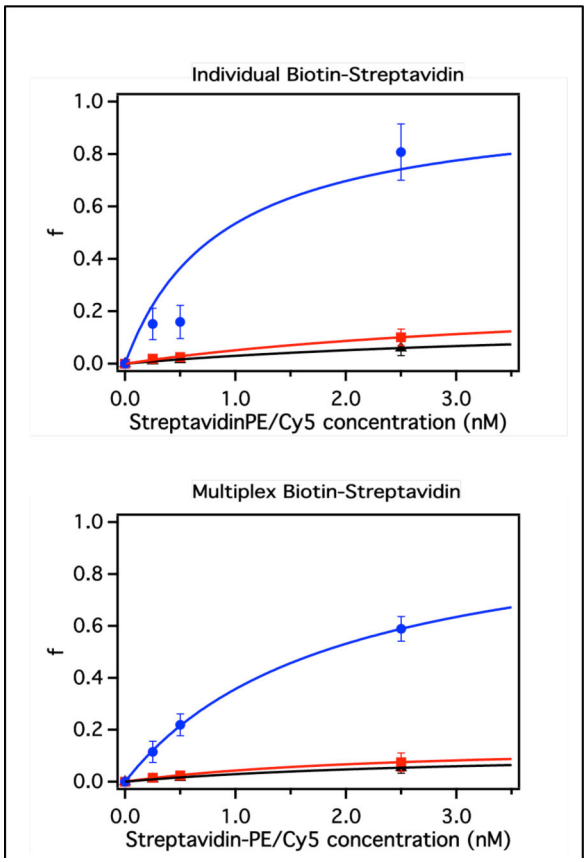

Figure 4.

Fractional binding of streptavidin (SAv-Cy5) after 10 minutes of incubation of samples containing lipids with 100% POPC + 0% Biotin (black, triangles), 99.75% POPC + 0.2% NBD-DOPE + 0.05% BiotinDOPE (red, squares) and 97.5% POPC + 2% NBD–DOPE + 0.5% Biotin-DOPE (blue, circles). The x-axis is increasing concentration of SAv-Cy5: 0 nM, 0.25 nM, 0.5 nM, and 2.5 nM. Data shown are the average of four replicates, and error bars are plus/minus one standard deviation. Solid lines are fits to the averaged data following the functional form of Equation (2), modified for streptavidin and biotin concentrations. The top panel presents results from the individual samples, and the bottom panel presents results from the multiplex system.

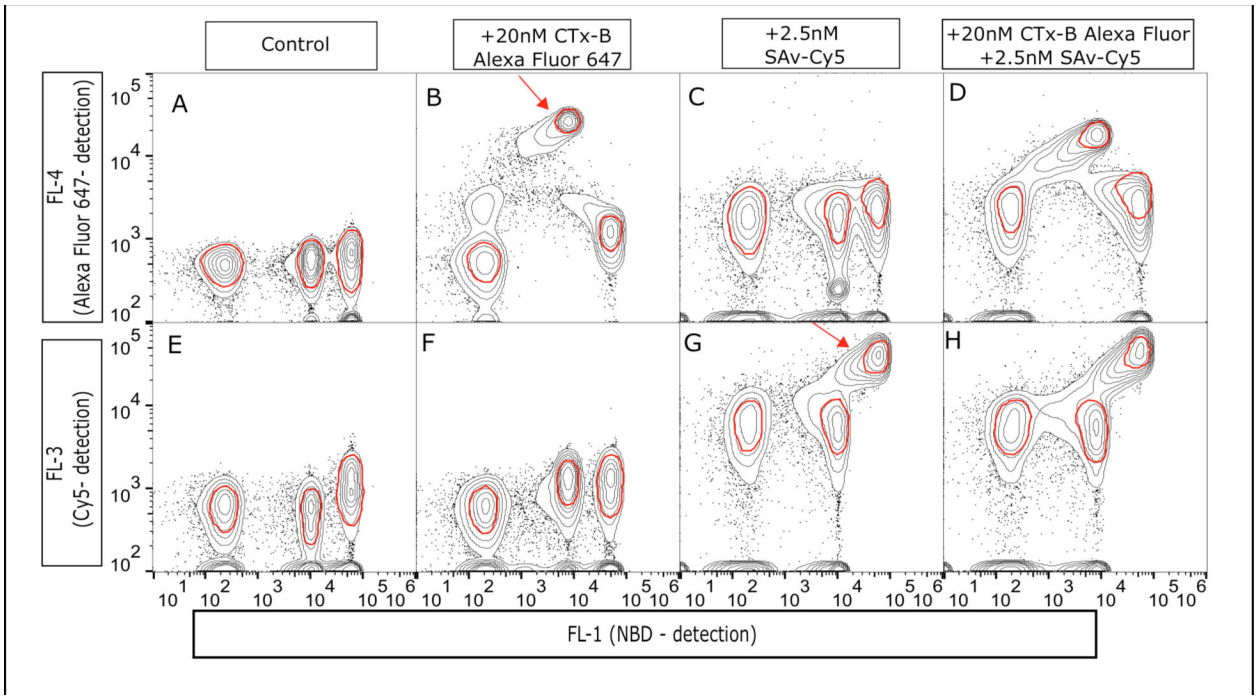

Figure 5.

Bivariate contour plots (FL-3 or FL-4 vs. FL-1) of the multiplexed samples: **A)** Control on FL-4. **B)** Plus 20 nM CTxB-Alexa 647 seen in FL-4. **C)** Plus 2.5 nM SAv-Cy5 seen in FL-4. **D)** Plus 20 nM CTxB-Alexa 647 and 2.5 nM SAvCy5 seen in FL-4. **E)** Control on FL-3. **F)** Plus 20 nM CTxB-Alexa 647 seen in FL-3. **G)** Plus 2.5 nM SAv-Cy5 seen in FL-3. **H)** Plus 20 nM CTxB-Alexa 647 and 2.5 nM SAv-Cy5 seen in FL-3.